Transport-Relevant Protein Conformational Dynamics and Water Dynamics on Multiple Time Scales in an Archetypal Proton Channel: Insights from Solid-State NMR

Transport-Relevant Protein Conformational Dynamics and Water Dynamics on Multiple Timescales in an Archetypal Proton Channel - Insights from Solid-State NMR

Journal:	*Journal of the American Chemical Society*
Manuscript ID	ja-2017-12464m.R1
Manuscript Type:	Article
Date Submitted by the Author:	n/a
Complete List of Authors:	Mandala, Venkata; Massachusetts Institute of Technology, Chemistry Gelenter, Martin; Massachusetts Institute of Technology, Department of Chemistry Hong, Mei; Massachusetts Institute of Technology, Department of Chemistry

Transport-Relevant Protein Conformational Dynamics and Water Dynamics on Multiple Timescales in an Archetypal Proton Channel - Insights from Solid-State NMR

Venkata S. Mandala, Martin D. Gelenter, and Mei Hong*

Department of Chemistry, Massachusetts Institute of Technology, 170 Albany Street, Cambridge, MA 02139

Revised for ***J. Am. Chem. Soc.***

Corresponding author: Mei Hong, Tel: 617-253-5521, Email: meihong@mit.edu

Abstract

The influenza M2 protein forms a tetrameric proton channel that conducts protons from the acidic endosome into the virion by shuttling protons between water and a transmembrane histidine. Previous NMR studies have shown that this histidine protonates and deprotonates on the microsecond timescale. However, M2's proton conduction rate is 10 – 1000 s^{-1}, more than two orders of magnitude slower than the histidine-water proton-exchange rate. M2 is also known to be conformationally plastic. To address the disparity between the functional timescale and the timescales of protein conformational dynamics and water dynamics, we have now investigated a W41F mutant of the M2 transmembrane domain using solid-state NMR. ^{13}C chemical shifts of the membrane-bound peptide indicate the presence of two distinct tetramer conformations, whose concentrations depend exclusively on pH and hence the charge-state distribution of the tetramers. High-temperature 2D correlation spectra indicate that these two conformations interconvert at a rate of ~400 s^{-1} when the +2 and +3 charge states dominate, which gives the first experimental evidence of protein conformational motion on the transport timescale. Protein ^{13}C-detected water ^{1}H T_2 relaxation measurements show that channel water relaxes an order of magnitude faster than bulk water and membrane-associated water, indicating that channel water undergoes nanosecond motion in a pH-independent fashion. These results connect motions on three timescales to explain M2's proton-conduction mechanism: picosecond-to-nanosecond motions of water molecules facilitate proton Grotthuss hopping, microsecond motions of the histidine sidechain allow water-histidine proton transfer, while millisecond motions of the entire four-helix bundle constitute the rate-limiting step, dictating the number of protons released into the virion.

Keywords

Magic-angle spinning NMR, conformational change, ion channel, exchange NMR

Introduction

Membrane-bound ion channels and transporters undergo conformational changes to conduct ions and transport substrates. The protein conformational changes can be triggered by membrane potential, pH, ligand concentration, mechanical activity, and even temperature [1]. The influenza A virus M2 protein is an acid-activated proton channel in the virus envelope [2-4]. M2 selects for protons using a conserved transmembrane (TM) histidine, His37 [5,6], and conducts protons asymmetrically from the N-terminus to the C-terminus using a conserved tryptophan, Trp41 [7,8].

The structure and dynamics of the influenza A virus M2 protein have been extensively studied using X-ray crystallography, solid-state NMR (SSNMR), solution NMR, and molecular dynamics simulations (for reviews, see [3,4,9]). These studies have focused on three aspects of M2's structure-function relation: the dynamic structures of the TM histidine and tryptophan, the backbone conformation of the four-helix bundle, and the water structures and dynamics in the channel. The first aspect is now relatively well understood. At low pH, the His37 imidazole ring undergoes microsecond-timescale protonation and deprotonation [10-12], ring reorientation [13] and tautomerization [14]. The protons are transferred between water and histidine, as shown by water-imidazole ^{1}H-^{15}N correlation NMR signals [11,15,16]. At both neutral and acidic pH, His37 adopts a *trans-trans* rotamer [13,17], which excludes interhelical N-H…N hydrogen bonding between two histidines [18]. Measured pK_a's of the four histidines of the tetramer indicate that the +3 charged channel has the highest proton conduction rate [10-12,16,19]. The Trp41 indole ring also undergoes microsecond-timescale reorientations at low pH, centered around an average sidechain conformation of t90 [20,21]. This motion periodically apposes the indole ring to the imidazolium ring, causing cation-π interactions that may curtail the number of protons released into the virion [20]. Mutation of Trp41 to Phe permits C-terminal protonation of His37 [16], while binding of the antiviral drug amantadine to Ser31 prevents N-terminal protonation of His37 [22-26].

Compared to the histidine and tryptophan structures, the backbone conformational dynamics and channel-water dynamics of M2 are not as well understood. Solid-state NMR chemical shifts and EPR data indicate that the TM domain is conformationally plastic in response to the membrane environment and pH [27-35]. Three discrete helix conformations have been captured in X-ray crystal structures [17,36,37]: a high-pH structure with a relatively open N-terminus and tightly packed C-terminus, a low-pH structure with a dilated C-terminus and a closed N-terminus, and an intermediate structure. MD simulations suggest that at least two of these conformations can interconvert in a transporter-like fashion for proton conduction [38]. Recent constant-pH MD simulations of M2TM in DMPC bilayers found that the pH dependence of protein conformation coincides with the pH dependence of proton conductance, supporting the notion that protein conformational changes may be required for channel activation [39]. However, to date, little direct evidence of protein conformational changes on the timescale of proton flux (10-1000 s^{-1}) [40-42] has been reported. Recent measurements of tryptophan fluorescence emission after laser-induced pH jump detected biphasic kinetics, where the slow rate of 4000 s^{-1} was assigned to conformational changes of M2 in DPPC/DHPC bicelles [43]. This rate is two orders of magnitude slower than the deprotonation rate of His37 but still faster than the proton conductance, leading the authors to conclude that conformational changes in the four-helix bundle are uncoupled from proton conduction.

Since water molecules in the channel both conduct protons through the Grotthuss mechanism and transfer protons to and from histidine, the abundance, location, hydrogen bonding and dynamics of channel water are important for understanding M2's proton conduction mechanism. ^{1}H spin diffusion

NMR spectra showed that the TM residues are much more water-accessible at low pH than at high pH [16,26,44], consistent with pore opening at low pH. Crystal structures of the TM domain [37] detected multiple structural water molecules in the pore. At 1.65 Å, two water clusters were observed above and below the histidine tetrad, suggesting that the cationic histidines may be stabilized by delocalization of the excess charge. At 1.10 Å, additional water molecules with partial occupancies outside the His-Trp region were observed, indicating the presence of multiple water wires from the channel entrance to the proton-selective histidine [37]. MD simulations suggest that these water molecules may switch their hydrogen-bonding directions in a charge-state dependent manner to allow Grotthuss hopping of protons. 2D IR spectra of the amide I transition of $^{13}C=^{18}O$ labeled Gly34 showed that water molecules proximal to Gly34 are rigid on the picosecond timescale at pH 8 but become dynamic at pH 6.2 [45], indicating that liquid-like water molecules flow into the channel at low pH. However, water dynamics on longer timescales and elsewhere in the channel have not been reported.

To further elucidate how protein backbone conformational motion and channel-water motion mediate proton conduction, we have now investigated a W41F mutant of M2 using solid-state NMR. The W41F mutant exhibits partial reverse proton current in voltage-clamp experiments [7] and permits protonation of His37 from the C-terminus, but it exhibits the same tetrameric assembly and backbone conformational behavior as wild-type M2 [16]. Here we show that the TM peptide exhibits two distinct tetramer conformations, as manifested by two sets of chemical shifts, whose intensities depend exclusively on pH. Importantly, high-temperature 2D ^{13}C-^{13}C correlation spectra indicate that these two tetramer conformations interconvert with a rate of ~400 s^{-1}, which represents the first experimental manifestation that the TM domain undergoes conformational motions on the proton transport timescale. We also characterized channel-water dynamics by measuring water ^{1}H T_2 relaxation times, and show that water in the M2 channel undergoes pH-independent nanosecond motions, in significant difference from IR-detected pH-dependent picosecond motions that have been assigned to hydrogen-bond breaking and reformation.

Materials and Methods

Peptide synthesis and membrane sample preparation

The W41F M2 transmembrane peptide (residues 22-46, SSDPLVVAASIIGILHLILFILDRL) was synthesized using Fmoc solid-phase synthesis protocol as detailed previously [16]. The VASGHD sample contains ^{13}C, ^{15}N-labeled V27, A30, S31, G34, H37, D44 and 4-^{19}F-labeled F41, while the VAGLI sample contains ^{13}C, ^{15}N-labeled V28, A29, G34, L38, and I39. Crude peptide was purified by reverse-phase HPLC on a Varian ProStar 210 System using a Vydac C18 column. The mass (2737.26 Da) and purity (>95%) were confirmed using MALDI-TOF mass spectrometry.

Purified peptide was reconstituted into a virus-mimetic lipid membrane (VM+) consisting of POPC, POPE, egg sphingomyelin and cholesterol at molar ratios of 25.6% : 25.6% : 25.6% : 23.2% [33,46]. The peptide and lipids were codissolved in organic solvents at a peptide : lipid molar ratio of 1 : 12 and lyophilized. The dry peptide-lipid mixtures were resuspended in buffers of desired pH, and vortexed and sonicated to obtain homogeneous vesicle solutions [16]. The solutions were spun down to obtain wet pellets, which were equilibrated to ~40 wt% water and packed into 3.2 mm MAS rotors for NMR experiments. VASGHD-containing membrane samples were prepared at pH 7.5, pH 6.2, pH 5.9, pH 5.5, and pH 4.5. Perdeuterated amantadine (d_{15}-Amt) was titrated to a pH 5.5 sample at a drug : tetramer ratio of 8 : 1. Three VAGLI-containing samples were prepared at pH 7.5, pH 5.5, and pH 5.5 with 8 : 1 d_{15}-Amt.

Solid-state NMR experiments and data analysis

Magic-angle-spinning (MAS) solid-state NMR spectra were measured on Bruker 600 MHz (14.1 Tesla), 800 MHz (18.8 Tesla) and 900 MHz (21.1 Tesla) spectrometers. Samples were spun at 10.5 kHz to 16 kHz. Typical radiofrequency (rf) field strengths were 50-71 kHz for ^{1}H, 35-60 kHz for ^{13}C, and 35-40 kHz for ^{15}N. ^{13}C chemical shifts were referenced externally to the adamantane CH_2 chemical shift at 38.48 ppm on the tetramethylsilane scale, while ^{15}N chemical shifts were referenced to the ^{15}N peak of N-acetylvaline at 122.0 ppm on the liquid ammonia scale. Sample temperatures are thermocouple-reported values.

2D ^{13}C-^{13}C Dipolar Assisted Rotational Resonance (DARR) and ^{15}N-^{13}C Transferred-Echo DOuble Resonance (TEDOR) experiments were measured to obtain ^{13}C and ^{15}N chemical shifts. The DARR mixing times were 100-150 ms and the TEDOR mixing times were 0.8-1.2 ms. 2D ^{13}C-^{13}C Proton-Driven Spin Diffusion (PDSD) experiment for long-range correlation was conducted at 800 MHz using a mixing time of 1.0 s. These 2D spectra were measured at 253 – 273 K. 2D ^{13}C-^{13}C correlation experiments for detecting conformational exchange were conducted using PDSD mixing at 298 – 308 K.

To study water dynamics, 1D ^{1}H and ^{13}C-detected spectra were measured at 800 MHz under 11 kHz MAS between 263 K and 293 K. These temperatures were thermocouple-reported values of the variable-temperature gas and are ~5 K lower than the sample temperature at 11 kHz MAS. The membrane samples were equilibrated at the target temperature for 1-3 hours before the spectra were measured.

For ^{1}H-detected water T_2 experiments (**Fig. S2a**), the ^{1}H Hahn-echo delay ranged from 0 to 550 ms. The hydrated proteoliposome samples used in this study have total sample masses of about 10 mg to 35 mg. Small-angle excitation-pulse tests indicate that the well-integrated hydration water does not cause radiation damping, since the water ^{1}H T_2 values are slightly shorter rather than longer with small excitation angles compared to T_2's measured using a 90° excitation pulse (data not shown). For ^{13}C-detected ^{1}H T_2 relaxation experiments (**Fig. S2b**), a Gaussian ^{1}H pulse of 1.25 – 1.5 ms was used to selectively excite water magnetization, followed by a 0.36 ms ^{1}H T_2 filter to remove residual rigid protein ^{1}H magnetization. The water ^{1}H magnetization was transferred to the protein protons using a variable mixing time, followed by 1 ms of cross polarization (CP) to ^{13}C for detection [26,44,47].

The pK_a values measured previously for His37 in W41F M2 allow the calculation of the charge state populations, N_i, as a function of pH [16]. The populations were fit to the measured pH-dependent C_{open} probability, $P(C_{open})$, using

$$P(C_{open}) = \sum_{i=0}^{+4} N_i \bar{p}_{i,C_{open}}, \quad (1)$$

which yields the time-averaged probability, $\bar{p}_{i,C_{open}}$, of the C_{open} conformation for each charge state. Best fit was obtained using a home-written Python code that minimized the chi square of the fit to the experimental data.

The ^{1}H T_2 relaxation data were fit using OriginPro and Matlab. The ^{1}H-detected relaxation data were fit to a stretched exponential function, $S/S_0 = e^{-(t/T_2)^{\beta}}$, where β ranges from 0 to 1. The ^{13}C-detected T_2 decays were fit to a single exponential function, $S/S_0 = e^{-t/T_2}$.

Results

M2 exhibits two tetramer conformations in the lipid membrane

We measured ^{13}C chemical shifts of W41F M2TM bound to a cholesterol-containing virus-mimetic membrane (VM+) [33,46] at different pH [16]. **Fig. 1** shows a representative 2D ^{13}C-^{13}C ^{1}H-driven spin diffusion (PDSD) spectrum, measured using a long mixing time of 1.0 s. At pH 5.5 with bound Amt. two sets of ^{13}C chemical shifts with similar intensities are resolved for all labeled residues, indicating two conformations with similar populations. One set of peaks, denoted as X, dominates at low pH, while the second set of peaks, denoted as Y, dominates at high pH (**Fig. 2**). With 1.0 s mixing, the 2D spectrum shows 41 inter-residue cross peaks, all of which are X-X or Y-Y but none of which are between X and Y. Spectra at other pH confirmed the absence of X-Y cross peaks. Interhelical cross peaks within a tetramer have been observed for His37 and other pore-facing residues of M2 before [10,13,48]. In the current sample, cross peaks such as A30 Cβ -G34 Cα and V27 Cα - S31 Cα are observed, and high-resolution crystal structures indicate that inter-helical distances between these residues are shorter (3.5 Å to 6.6 Å) than intra-helical distances (4.5 Å to 6.7 Å) (**Fig. S1**), thus many X-X and Y-Y cross peaks are mainly inter-helical in origin. These results indicate that all four helices within a tetramer adopt the same conformation, and the X and Y conformations result from different tetramers. The relative intensities of the X peaks increase with decreasing pH for all residues, indicating that entire four-helix bundles convert from the Y conformation to the X conformation as the pH decreases. This pH-dependent conformational duality is fundamentally different from the previously reported dimer-of-dimer structure for an amphipathic-helix-containing construct of M2 [34], where two sets of chemical shifts with equal intensities show cross peaks between them, indicating that two conformations coexist within each tetramer. This breaking of the tetramer symmetry may be caused by the curvature-inducing ability of the amphipathic helix [49-52], the negative-curvature diphytanoyl-phosphocholine membrane [53,54], and other experimental conditions used in that study.

The two conformations correlate with pH and the tetrad charge state

The nature of the X and Y conformations can be elucidated by examining the pH dependence of their intensities. **Fig. 2** shows regions of the 2D ^{13}C-^{13}C and ^{15}N-^{13}C correlation spectra for the six labeled residues. The spectra were measured at low temperature (253-273 K) to freeze out conformational motion. The Y resonances dominate at high pH while the X peaks dominate at low pH. At intermediate pH, both sets of peaks have significant intensities, indicating that the two states are near equilibrium, but no intermediate chemical shifts are present, confirming the bimodal nature of the conformational distribution. Based on this pH dependence and the known crystal and SSNMR structures, we assign the high-pH Y chemical shifts to a C_{closed} conformation and the low-pH X chemical shifts to a C_{open} conformation. Chemical shifts, linewidths, and orientational data [25] indicate that the low-pH C_{open} conformation has relatively straight helices [28] while the high-pH C_{closed} conformation contains a small kink at Gly34.

The two-state equilibrium is best seen at pH 5.5 to 5.9, where A30 Cβ, S31 Nα, and G34 Cα show chemical shifts that are resolved by 1.3 – 3.0 ppm. V27 Cβ and Nα show smaller chemical shift differences between X and Y states, while the D44 Cβ peak moves upfield with decreasing pH. The

D44 Cβ linewidth also decreases significantly at pH 4.5, suggesting that carboxyl protonation creates a more homogeneous structure. Drug binding narrowed the linewidths of all residues compared to the apo sample, indicating increased structural homogeneity.

We quantified the populations of the C_{open} (X) and C_{closed} (Y) conformations as a function of pH using integrated intensities of A30 Cβ, S31 Nα and G34 Cα peaks and the chemical shift of D44 Cβ (**Fig. 3a-d**). The average C_{open} population decreases from ~90% at pH 4.5 to ~20% at pH 7.5, while the average C_{closed} population increases from ~10% at pH 4.5 to ~80% at pH 7.5. Interestingly, the C_{open} fraction shows a moderate dependence on the residue position: C-terminal residues exhibit a higher C_{open} population at low pH compared to N-terminal residues (**Fig. 3e**). The majority of the conformational transition occurs between pH 4 and 6; outside this range, the populations of the C_{open} and C_{closed} states are largely constant.

In principle, each charge state of the channel can have different propensities for the C_{open} and C_{closed} conformations. To investigate this charge-state dependence of the conformation, we considered the total X and Y populations as the population-weighted average of the individual charge-state's C_{open} and C_{closed} conformations. The four pK_a's of the His37 tetrad in W41F M2TM have been recently measured to be 6.7, 6.3, 5.8, and 5.1 [16], which give the populations of the charge states (**Fig. 3f**). The +3 charge state peaks at pH 5.5, while the +2 charge state reaches maximum population at pH 6.2. The rapid increase of the C_{open} conformation below pH 6 correlates with the increased +3 population. Fitting the average C_{open} fractions (**Fig. 3g**) using the charge-state populations yielded the time-averaged probability of the C_{open} conformation ($\overline{p}_{i,C_{open}}$) for each charge state (**Fig. 3h**). The +3 state and +4 state have the highest C_{open} probabilities of 85 ± 10% and 95 ± 3%, while the +0, +1 and +2 charge states have much lower C_{open} probabilities of 17 ± 2%, 19 ± 3%, and 22 ± 4%, respectively. The C_{open} probabilities of each charge state also allowed us to calculate the free-energy difference, ΔG_i°, between the C_{open} and C_{closed} states (**Fig. 3i**), according to

$$\Delta G_i^\circ \equiv G_{open,i}^\circ - G_{closed,i}^\circ = -RT\, ln \frac{\overline{p}_{i,C_{open}}}{\overline{p}_{i,C_{closed}}} \qquad (2)$$

The C_{closed} state is favored by 3.5 ± 0.3, 3.2 ± 0.4, and 2.8 ± 0.4 kJ/mol over the C_{open} state when the His37 tetrad has an excess charge of +0, +1 and +2, respectively, while the C_{open} state is favored by 3.8 ± 0.3 and 6.4 ± 0.1 kJ/mol when the tetrad occupies the +3 and +4 charge states, respectively. Therefore, the C_{open} probability increases 4-fold when the +2 state converts to the +3 state, which supports previous results that proton conduction is mediated by the +2 to +3 transitions of the His37 tetrad [10,39].

The two tetramer conformations interconvert on the millisecond timescale at high temperature

To investigate whether the C_{open} and C_{closed} conformations interconvert on the proton conduction timescale [38], we measured 2D ^{13}C-^{13}C correlation spectra of the membrane-bound M2TM at high temperature (298 - 308 K) (**Fig. 4**). To maximize the chance of detecting conformational exchange, we chose samples at intermediate acidic pH where the C_{open} and C_{closed} conformations are both present at significant populations (**Fig. 3g**). **Fig. 4a** shows the spectra of the pH 5.9 VASGHD sample. Importantly, the X and Y chemical shifts of A30 Cβ, G34 Cα and G34 C′ are averaged at 298

K. The line narrowing is particularly apparent when compared to the 263 K spectrum, which shows well resolved X and Y chemical shifts for these sites. Thus, at 298 K, conformational exchange occurs at a rate comparable to or slightly faster than the chemical shift differences of 2 ppm or ~400 s^{-1}, given the ^{13}C Larmor frequency of 200 MHz. Since the +2 and +3 charge states have the highest populations among all charge states at pH 5.9 (**Fig. 3f**), this chemical shift averaging correspond to conformational changes between the predominantly C_{closed} +2 state and the predominantly C_{open} +3 state (**Fig. 3h**).

To understand the residual non-averaged intensities, we measured the 2D correlation spectra of the pH 5.5 VAGLI sample. This sample shows stronger G34 Y peaks than X peaks (**Fig. 4b**), and generally have similar intensity distributions to those of the pH 6.2 VASGHD sample, indicating that this pH 5.5 VAGLI sample has a higher effective pH and thus should contain a large population of +1 and +2 charge states. We chose this sample to look for slow-exchange cross peaks since it has higher sensitivity than other samples with low charge states. **Fig. 4b** shows that at 308 K, exchange cross peaks between G34 Cα X and Y chemical shifts and between G34 carbonyl X and Y chemical shifts are indeed present by a mixing time of 0.2 s. The cross peak intensities are ~25% of the intensities of the parent peaks, and disappear at 273 K even when a long mixing time of 1.0 s was used, thus proving that the high-temperature cross peaks result from conformational dynamics, whose rates are on the order of ~1 s^{-1}. Therefore, conformational changes between C_{open} and C_{closed} states also occur in low charged channels, but they are at least an order of magnitude slower than the proton conduction rates of 10-1000 s^{-1} and thus do not contribute to function.

Drug binding to the pH 5.5 VASGHD sample abolished both chemical shift averaging and slow-exchange cross peaks (**Fig. 4c**), and returned the same well resolved X and Y chemical shifts at both high and low temperatures, indicating that drug binding arrests the protein conformational change.

Heterogeneous water environments in M2-containing proteoliposomes

We next turned to an investigation of the channel-water dynamics, by detecting water ^1H spectra (**Fig. 5**) and ^1H T_2 relaxation times (**Fig. S2a**) as a function of pH and temperature. At high temperature (293 K), a single water ^1H peak between 4.78 and 4.81 ppm is observed at most pH, indicating that all water molecules associated with the membrane undergo fast translational and rotational diffusion at this temperature. The only exceptions are the pH 7.5 samples, which show two resolved ^1H signals: the narrow peak at 4.79 ppm with a T_2 relaxation time of 54.4 ms can be assigned to bulk-like water while the broad peak at 4.83 ppm with a shorter T_2 relaxation time of 13.0 ms can be assigned to membrane-associated water. This broad peak is absent in protein-free samples at the same pH (**Fig. S3b**), suggesting that the closed state of M2 causes a heterogeneous environment in which one fraction of water is tightly bound to the membrane, distinct from the bulk water.

As the temperature decreases, the water ^1H spectra of the pH 7.5 and 5.9 samples resolve at least two peaks while the spectra of the lower pH samples are broadened. At 263 K, the water signals of the two high-pH sample show a chemical shift difference of 55 Hz and 65 Hz, indicating that the two water populations do not exchange on the timescale of ~20 ms at this temperature. The downfield water peak at 5.20 ppm has a longer T_2 relaxation time of 79.5 ms and 118.3 ms at pH 7.5 and pH 5.9, respectively, while the upfield ^1H signal at 5.12 ppm has a shorter T_2 relaxation time of 61.5 ms at both pH 7.5 and 5.9. Thus we assign the downfield ^1H signal to bulk-like water and the upfield peak to membrane-associated water. Similar doublet water spectra have been previously observed in

microcrystalline proteins [55] and amyloid fibrils [56], and can be attributed to bulk-like water in slow exchange with protein-interacting water.

For W41F M2TM, the doublet pattern is pH-dependent: the feature disappears at pH 5.5, and is replaced by a single broad peak with a short T_2 of 17.8 ms (**Fig. 5c**), indicating that the bulk-like water undergoes fast exchange with lipid- and protein-associated water. To investigate whether this exchange is caused by M2 or the lipid membrane, we measured the ^{1}H spectra and T_2 relaxation times of protein-free control membranes. **Fig. S3** shows that the control samples retain the two-peak lineshapes at pH 5.5 and pH 6.2, similar to the high pH samples, and the water T_2 relaxation times range from 59.0 ms to 122.7 ms. Therefore, the single water ^{1}H peak for the M2-containing membranes at low pH can be attributed to protein-induced averaging of water dynamics. At pH 5.5, the dominant charge state of W41F M2TM is +3, while the dominant charge states at pH 5.9 and pH 7.5 are +2 and +0, respectively [16]. Therefore, we propose that the conducting +3 state at pH 5.5, together with significant populations of the +2 and +4 states, cause a rough membrane surface that may disrupt the hydrogen-bonding network of water on the membrane surface, thus facilitating water exchange. Finally, the drug-bound samples at pH 5.5 give similarly unresolved water ^{1}H spectra (**Fig. 5d,e**), but show distinct T_2 relaxation times across the lineshape, indicating that the water ^{1}H peak is inhomogeneously broadened. This suggests that drug binding slows down the water exchange and gives rise to at least two distinct water environments.

Fast chemical exchange of water at high temperature and slow dynamics of the channel water

The water ^{1}H T_2 relaxation times in **Fig. 5** were measured using ^{1}H Hahn echo experiments (**Fig. S2a**). The observed decays are not single exponential, indicating heterogeneous water environments in these membrane samples. In general, at least three types of water molecules can be distinguished: bulk-like water between bilayers, water that is tightly associated with the lipid headgroups on the membrane surface, and water in the channel. At the hydration level of 30-45 wt% used for our membrane samples, based on a 2 nm thickness for the interlamellar water layer [57], the protein : lipid molar ratio of 1 : 12, and assuming 32 water molecules in each channel based on the recent high-resolution crystal structure [37], we estimate that ~30% of the total sample mass corresponds to the interlamellar water while only ~3% of the sample mass is channel water. For well-hydrated, multilamellar POPC vesicles, the number of water molecules bound to each lipid headgroup is 9.4, while the number of interlamellar water molecules associated with each lipid is 31.0 [57]. Thus, ~30% of the interlamellar water interacts significantly with lipid headgroups, while the remaining water is more bulk-like. Given this heterogeneity, the non-exponential decay of the T_2 relaxation is expected. We thus fit the echo intensities using stretched exponential functions. The exponent β was found to range from 0.64 to 1.10 (**Table S1**).

Importantly, at all pH, the ^{1}H T_2 relaxation times (10.0 to 54.4 ms) are the shortest at high temperature and increase at low temperature (17.8 to 118.3 ms) (**Tables S2**), in contrast to the temperature dependence expected from the classical Bloembergen-Purcell-Pound (BPP) theory [58]. This indicates that the bulk-like water undergoes rapid translational diffusion and chemical exchange with membrane-associated water at high temperature, which shortens the T_2. At low temperature this diffusion and chemical exchange slow down, thus lengthening the T_2 values.

Since channel water represents only ~7% of all water in these hydrated membranes, we next probed the dynamics of the channel water close to the protein residues by indirect ^{13}C-detection of the

water ^{1}H T_2 relaxation times. The water ^{1}H magnetization was selectively excited using a 1.25-1.50 ms Gaussian pulse, allowed to decay during an echo period, then transferred to the protein protons and detected through protein ^{13}C signals (**Fig. S2b)** [44]. Previous studies of membrane-bound M2TM showed that ^{1}H spin diffusion mixing times of 4-16 ms are sufficient for localizing the magnetization to protein-proximal water [26,56]. We found that spectra measured with 16 ms and 4 ms ^{1}H-^{1}H mixing times gave the same T_2's (**Fig. S4**), thus we used 16 ms to increase the spectral sensitivity. **Fig. 6** shows that the ^{13}C-detected water ^{1}H T_2's decay in a single-exponential fashion, indicating homogeneous dynamics of the channel water. Interestingly, the ^{13}C-detected ^{1}H T_2 values (**Table S3**) are an order of magnitude shorter than the ^{1}H-detected T_2 values, indicating that the channel water is much more immobilized than bulk water, and the channel water has minimal chemical exchange with the interlamellar water. Drug binding to the channel further shortened the ^{1}H T_2's compared to the apo sample (**Fig. 6d**), indicating that the channel water becomes even more immobilized and isolated from the interlamellar water in the drug-bound state.

Discussion

These results provide novel insights into how protein conformational motion and water motion mediate proton conduction through the M2 channel. We observed two conformations for the membrane-bound W41F M2TM: the X conformation dominates at low pH while the Y conformation is prevalent at high pH. The two sets of chemical shifts for W41F M2 qualitatively agree with and extend beyond previous data on wild-type M2 [28,33]. The absence of X-Y cross peaks at low temperature indicates that these two conformations are well separated in space, and result from two tetramer populations rather than from two monomer conformations within a tetramer. Importantly, at high temperature, X-Y chemical shift averaging indicates that the two conformations interconvert at a rate of ~400 s^{-1} at a pH where the +2 and +3 charge states are prevalent. This result provides the first experimental evidence for a transporter-like mechanism, where large-scale cooperative changes of the TM helix conformation between the C_{open} and C_{closed} states occurs on the millisecond timescale and corresponds to the rate-limiting step in proton conduction [38,40-42]. When lower charge states (+1 and +2) dominate, conformational exchange still occurs but slows down to ~1 s^{-1}, thus this motion does not contribute to proton conduction.

The bimodal (C_{open} and C_{closed}) conformational distribution is intimately related to the charge state (0, +1, +2, +3 and +4) distribution of the protein. The pH-dependence of the C_{open} and C_{closed} populations indicate that channel opening is favored greatly by a highly charged His37 tetrad. The +3 and +4 charged channels have 4-fold higher C_{open} probabilities than the lower charge states. Interestingly, the probability of the C_{open} conformation is non-zero even in the fully neutral channel. This is consistent with previous observation of a minor population of C_{open} conformation at pH 8.5 in wild-type M2TM [28], and indicates that a small population of the C_{open} state at high pH may be important for channel activation at low pH.

We can gain further insight into the equilibrium constants defining the stability of the C_{closed} and C_{open} conformations in each charge state by using the measured relative intensities of the X and Y peaks at different pH. Assuming that the two conformations for each charge state *i* are at equilibrium,

$$C_{closed,\,i} \underset{k_{close,\,i}}{\overset{k_{open,\,i}}{\rightleftharpoons}} C_{open,\,i}, \qquad (3)$$

then the rate constants for channel closing and opening are related to the equilibrium constant for the conformational change in the i^{th} charge state according to:

$$K_{conf,\,i} \equiv \frac{\left[C_{open,\,i}\right]}{\left[C_{closed,\,i}\right]} = \frac{k_{open,\,i}}{k_{close,\,i}} \tag{4}$$

The relative intensities of the C_{open} and C_{closed} states in the spectra allow us to determine the pH-dependent K_{conf} (pH), from which the Gibbs free energy difference between the open and closed conformations can be calculated according to

$$\Delta G^{\circ}(pH) \equiv G^{\circ}_{open} - G^{\circ}_{closed} = -RT\ln K_{conf}\left(pH\right) = \sum_{i=0}^{+4} N_i\left(pH\right)\Delta G_i^{\circ}. \tag{5}$$

Thus, the pH-dependence of K_{conf} and ΔG° arises from the pH-dependence of the His37 charge-state population N_i. Using the average C_{open} fraction for A30, S31 and G34 (**Fig. 3g**), we found that at 273 K, the C_{closed} conformation is favored by 3.2 kJ/mol at pH 7.5 while the C_{open} conformation is favored by 5.6 kJ/mol at pH 4.5 (**Fig. 7a**). At pH 5.8, the two conformations have equal free energies.

At pH 5.9, the spectral intensities show $K_{conf} = 0.7$, indicating that k_{open} is 0.7-fold smaller than k_{close}. The conformational exchange rate of ~400 s^{-1} at 298 K measured from the 2D spectra represents the slower of the two rate constants, implying that k_{close} is about 550 s^{-1} and k_{open} is about 400 s^{-1} at this pH. At pH lower than 5.8, the C_{open} state is favored over the C_{closed} state, indicating a smaller K_{conf}. This decrease may be due to an increase in k_{open}, a decrease in k_{close}, or a combination of the two. Since the +3 state is the minimum charge state required to promote the C_{open} conformation, the rate constant for channel opening likely increases with proton concentration. Meanwhile, k_{close} is associated with His37 deprotonation, which increases with decreasing pH due to the excess positive charge at the His37 tetrad [21]. Thus, the rate of conformational interconversion in both directions may increase at pH lower than 5.8, but the increase in k_{open} dominates over the increase in k_{close}, thus shifting the equilibrium towards the C_{open} conformation. The equilibrium plateaus below pH 4 because the rate of deprotonation and protonation at His37 saturates once the tetrad is fully protonated (at pH ~3.5), beyond which increasing the proton concentration has little effect on proton dissociation and association.

Is the pH-dependent millisecond conformational motion specific to the W41F mutant or is it also present in naturally occurring M2 sequences with the intact HxxxW motif? Previous spectra of wild-type M2TM bound to single-component phosphocholine membranes, DLPC and DMPC, and a rigid viral membrane (VM) mixture in which DPPC and DPPE were used in place of POPC and POPE, showed the same pH-dependent chemical shift doubling for G34, S31 and V27 [28] as seen in the W41F mutant. Thus, the condition exists for slow conformational exchange. However, high-temperature conformational exchange of wild-type M2TM could not be measured in DLPC and DMPC membranes due to uniaxial diffusion of the entire four-helix bundle in these bilayers [59,60], while high-temperature spectra of VM-bound M2TM did not show chemical shift averaging [10], likely due to the high viscosity of the VM membrane compared to the VM+ membrane [33,61]. Thus, millisecond-timescale motions have

not been investigated in wild-type M2 in a membrane environment that is conducive to its detection. Since the W41F mutant conducts protons 1.7-4.0 times faster than wild-type M2 [6], and conformational exchange in W41F M2 occurs at ~400 s^{-1}, we expect the backbone conformational exchange to be present in wild-type M2 but at a slower rate of 50-250 $^{s-1}$, which is still within the range of proton conduction rate of 10-1000 s^{-1}. This expectation is supported by the S31N mutant, which contains the HxxxW motif and which exhibits pH-dependent proton conductance that is only 1.5-2.0 times that of wild-type M2 [6]. Two L38 Cα-Cβ cross peaks were resolved at low temperature in S31N-M2, and at high temperature the Cβ chemical shift is averaged over a frequency difference of ~350 Hz (**Fig. 4d**) [14] [14]. Thus, the HxxxW-intact S31N M2 also undergoes millisecond motion, strongly suggesting that the transporter motion is present in wild-type M2. Moreover, the exchange rates may have a simple linear correlation with the proton conductance.

Channel water dynamics on the nanosecond timescale

High-resolution crystal structures have detected well-defined water clusters in M2 at cryogenic temperatures [17,37], and MD simulations have predicted the existence of well-ordered channel water that relays protons to His37 [62,63]. However, relatively little experimental data have been reported so far about the dynamics of channel water at physiologically relevant temperatures and membrane conditions. Our ^{13}C-detected ^{1}H T_2 data indicate that water has surprisingly slow motions in the M2TM channel. The channel water represents only ~7% of the total water in these hydrated proteoliposome samples, and is thus masked by the dominant membrane-associated and bulk-like interlamellar water in the ^{1}H spectra. ^{13}C detection is therefore essential for reporting the dynamics of protein-proximal channel water. At 263 K, the ^{13}C-detected water ^{1}H T_2's range from 2.9 to 7.4 ms, which are an order of magnitude shorter than the ^{1}H-detected T_2's of 18 - 118 ms for membrane-surface water and interlamellar bulk-like water (**Fig. 6d**). The millisecond T_2 values of the channel water correspond to molecular correlation times of 6-15 ns [58]. Moreover, the ^{13}C-detected water T_2's are relatively independent of pH, in contrast to the pH-dependence of the protein conformational dynamics. We hypothesize that the relatively slow motion of these channel-water molecules may facilitate proton hopping via the Grotthuss mechanism to and from His37.

Interestingly, the pH-independence of the nanosecond motion of channel water differs from the picosecond dynamics of water detected from 2D IR spectra [45]. Measurement of the G34 $^{13}C=^{18}O$ amide I transition found distinct spectral lineshapes and dynamics at high and low pH: at pH 8.0, the spectra show a single band that remains constant over several picoseconds, while at pH 6.2, two intense bands were observed that change with a correlation time of 1.3 ps. These spectral differences were attributed to different water dynamics around the G34 amide group: at high pH water is immobilized on the picosecond timescale, while at pH 6.2, water near G34 is liquid-like and breaks and remakes hydrogen bonds on the picosecond timescale.

Drug binding shortened the water ^{1}H T_2's further compared to the apo channel (**Table S3**), indicating additional slowing of channel-water dynamics. MD simulations have suggested that the amine group of amantadine is solvated by water molecules [64], thus providing a rationale of the water ordering and the shorter T_2's in the presence of bound drug. The drug-bound VAGLI sample has longer T_2's than the drug-bound VASGHD sample (**Fig. 6d**), which can be attributed to incomplete drug binding to the VAGLI sample. This is supported by the fact that the linewidths of the VAGLI sample do not differ significantly between the drug-bound and *apo* states, in contrast to the clear line narrowing seen for the drug-bound VASGHD sample (**Fig. S5**).

Conclusion

The solid-state NMR data shown here, together with previous NMR studies of the sidechain motions of His37 and Trp41 and IR studies of water dynamics, give the fullest account to date of how molecular motions over ten orders of magnitude combine to lead to proton conduction through this archetypal channel. On the picosecond timescale, water undergoes small-amplitude motion that breaks and remakes hydrogen bonds at low pH but not at high pH. Channel water also exhibits slow, nanosecond-timescale motion, independent of pH, which may facilitate Grotthuss hopping of protons over the water wire to the proton-selective His37. The His37 imidazole ring undergoes microsecond-timescale reorientational motion at low pH, in synchrony with histidine-water proton exchange. However, most of these proton exchange events are futile; only when a majority of the tetramers are in the +2 and +3 charge states does the entire TM four-helix bundle undergo cooperative conformational changes from a C_{closed} structure to a C_{open} structure to allow proton release. This conformational change occurs at a rate of ~400 s^{-1} at 298 K when M2 is bound to cholesterol-containing lipid bilayers. The charge-state requirement for detecting this conformational change results from the fact that the low-charge tetramers (0, +1, +2) predominantly adopt the C_{closed} conformation while the high-charge tetramers (+3 and +4) mainly adopt the C_{open} conformation, thus interconversion can only be easily observed between +2 and +3 charge states. The charge state of the channel has a direct impact on the relative populations of the C_{open} and C_{closed} conformations. For lower charge states, conformational changes still occur between the C_{open} and C_{closed} states, but with a much slower rate of ~1 s^{-1}, thus they do not contribute to proton conduction. Therefore, proton conduction in the M2 channel requires picosecond and nanosecond water dynamics for Grotthuss hopping, microsecond His37 sidechain reorientations for histidine-water proton transfer, and finally, millisecond cooperative protein backbone motions that dictate the number of protons that are successfully released into the virion.

Supporting Information Available:

Additional tables and NMR spectra include:
^{1}H and ^{13}C-detected water ^{1}H T_2 relaxation times (Tables S1-S3)
Intra-helical and inter-helical distances in the transmembrane domain of M2 (Figure S1)
Pulse sequences for measuring water ^{1}H T_2 relaxation times (Figure S2)
Water ^{1}H MAS spectra (Figure S3)
^{13}C-detected water ^{1}H T_2 relaxation decays (Figure S4)
^{13}C spectra showing effects of amantadine binding on the Cα linewidths (Figure S5).

This material is available free of charge via the Internet at http://pubs.acs.org.

Acknowledgements

This work is supported by NIH grant GM088204 to M.H.

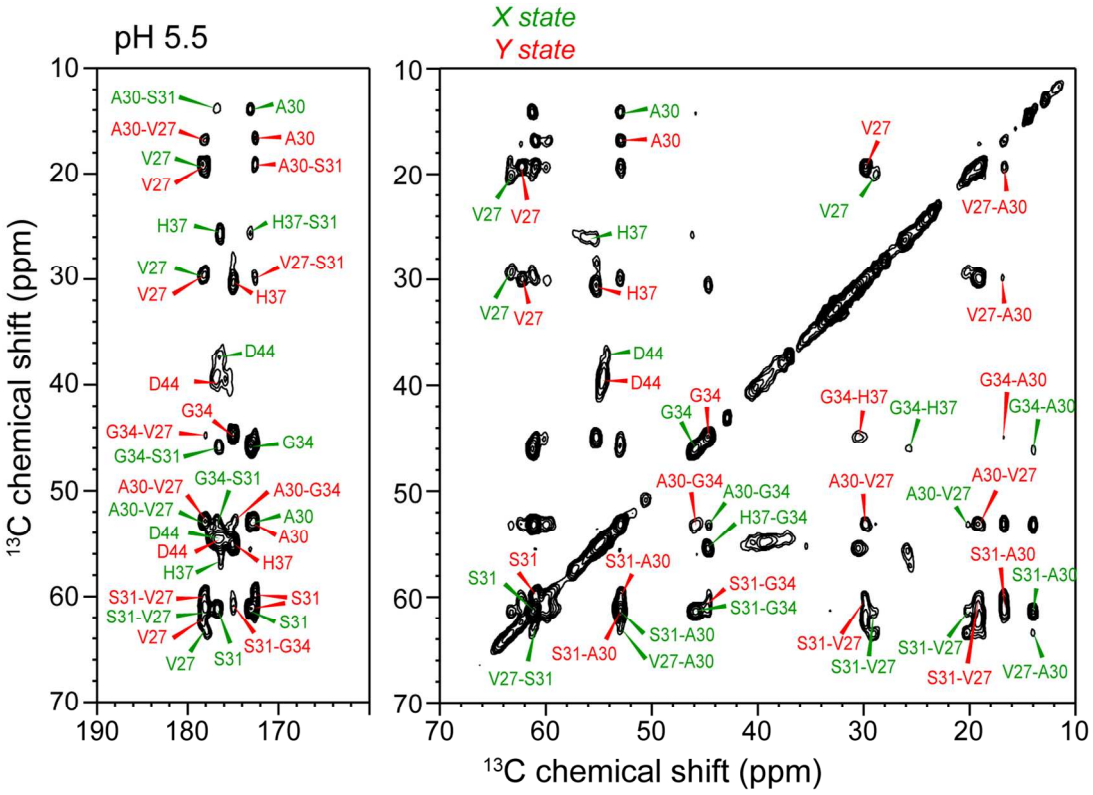

Figure 1. 2D ^{13}C-^{13}C PDSD spectrum of VASGHD-labeled W41F M2TM at pH 5.5 with bound amantadine. The spectrum was measured using a spin diffusion mixing time of 1.0 s at 263 K under 14.5 kHz MAS on an 800 MHz spectrometer. Most residues show two sets of chemical shifts, which are assigned in green (type X) and red (type Y). Only X-X and Y-Y cross peaks are seen while no X-Y cross peaks are detected. For clarity, intra-residue cross peaks are assigned on the top left while inter-residue cross peaks are assigned on the bottom right.

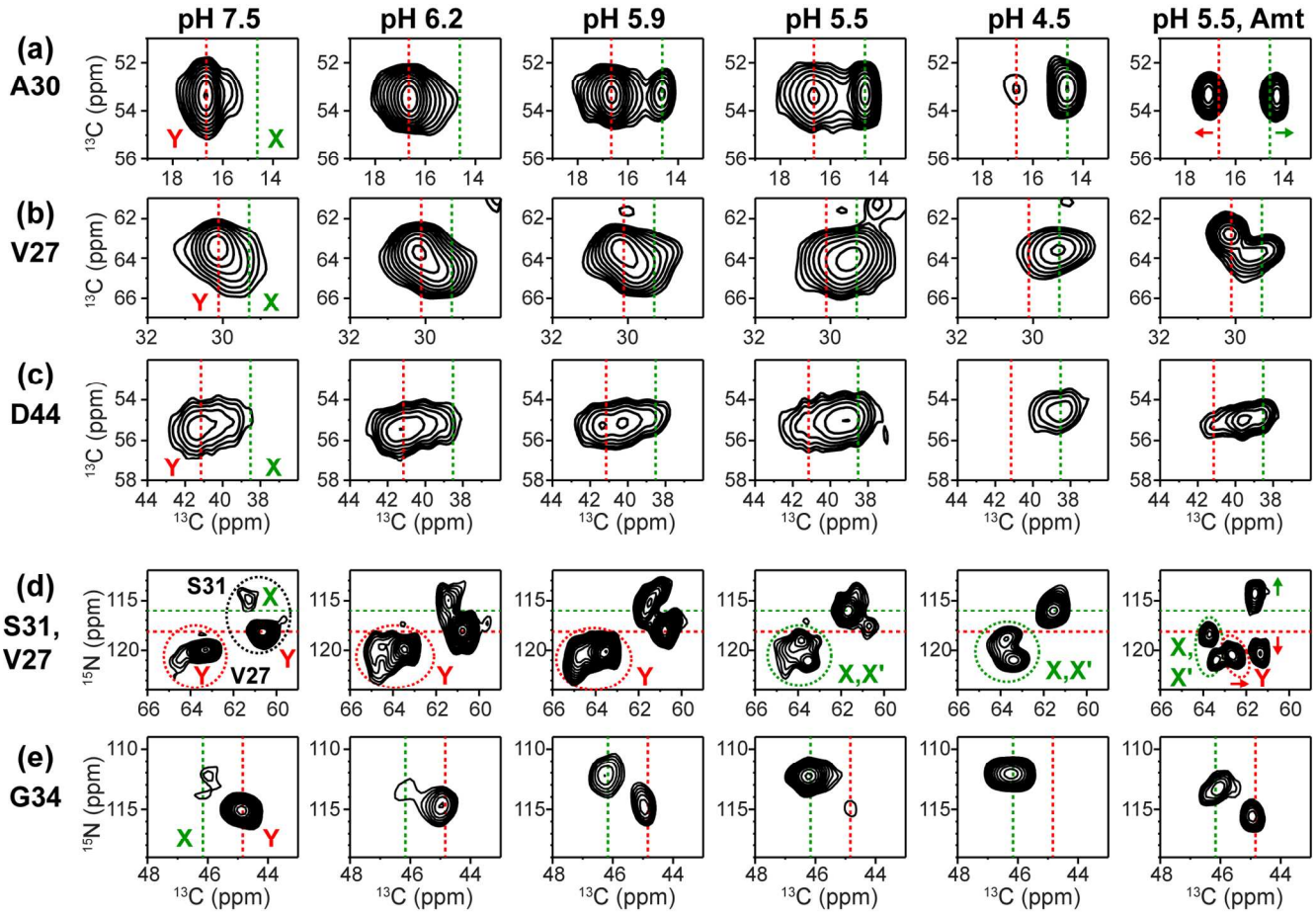

Figure 2. pH dependence of the intensities of the X and Y cross peaks of key TM residues in 2D ^{13}C-^{13}C (a-c) and ^{15}N-^{13}C (d-e) correlation spectra of VASGHD-labeled W41F M2TM. (a) A30. (b) V27. (c) D44. (d) V27 and S31. (e) G34. V27 shows additional peaks in the ^{15}N-^{13}C correlation spectra. Amantadine (Amt) binding at pH 5.5 significantly narrowed the linewidths, better resolving the X and Y peaks, and increased the Y peak intensities compared to the apo sample at pH 5.5. Arrows denote chemical shift changes due to Amt binding.

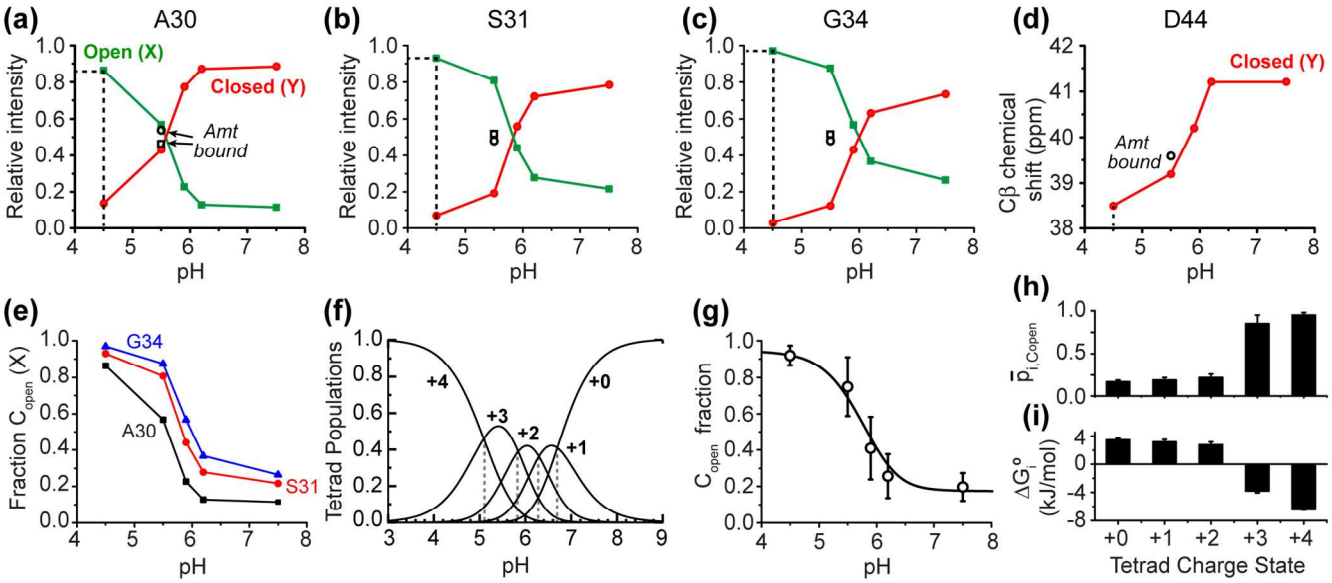

Figure 3. pH dependence of M2 conformational equilibrium and its relation to the tetrad charge state. (a-d) pH-dependent intensities and chemical shifts of the C_{open} (X) and C_{closed} (Y) peaks. Relative integrated intensities are shown for (a) A30, (b) S31 and (c) G34. (d) Chemical shift of the D44 Cβ peak as a function of pH. (e-i) Relation between the His37 tetrad charge state and conformational equilibrium of W41F M2TM. (e) Fraction of the C_{open} (X) conformation for TM residues obtained from (a-c). The N-terminal residues show lower C_{open} probabilities than the C-terminal residues. The mid point of the conformational change is pH 5.8, similar to the average pK_a (6.0) of the channel. (f) Populations of the different tetrad charge states as a function of pH, calculated using the pK_a's of W41F M2TM [16]. (g) Probability of the C_{open} conformation averaged over all residues and the best fit using eq. (1). (h) Time-averaged probability of the C_{open} conformation of the five charge states of the channel. (i) Gibbs free energy difference between the C_{open} and C_{closed} conformations for the five charge states of the channel.

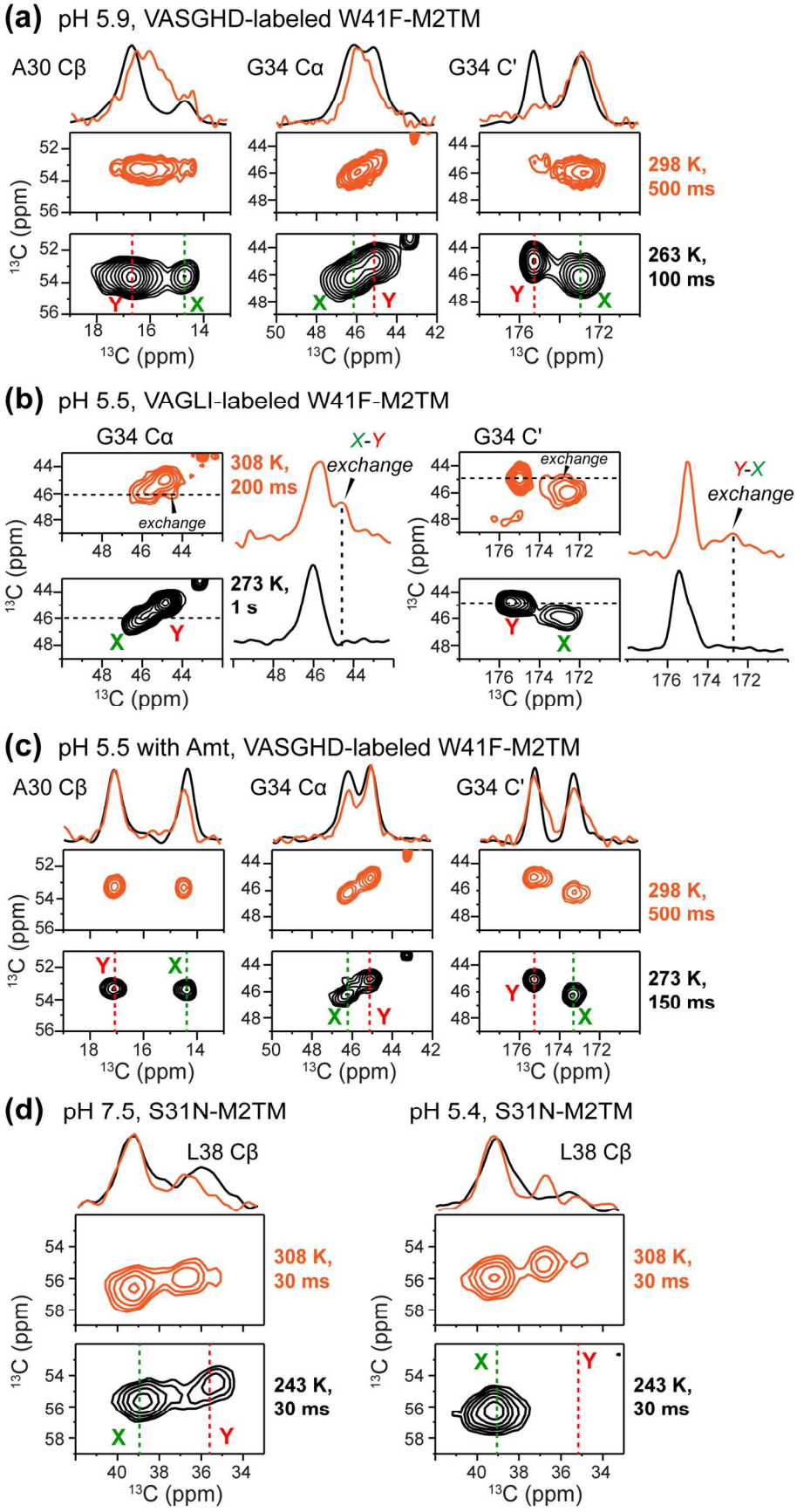
(a) pH 5.9, VASGHD-labeled W41F-M2TM
A30 Cβ
G34 Cα
G34 C'
298 K, 500 ms
263 K, 100 ms
^{13}C (ppm)
(b) pH 5.5, VAGLI-labeled W41F-M2TM
G34 Cα
G34 C'
308 K, 200 ms
273 K, 1 s
X-Y exchange
Y-X exchange
exchange
(c) pH 5.5 with Amt, VASGHD-labeled W41F-M2TM
A30 Cβ
G34 Cα
G34 C'
298 K, 500 ms
273 K, 150 ms
(d) pH 7.5, S31N-M2TM
pH 5.4, S31N-M2TM
L38 Cβ
308 K, 30 ms
243 K, 30 ms

Figure 4. 2D ^{13}C-^{13}C PDSD spectra at high and low temperatures reveal millisecond motions in (a-c) W41F-M2 and (d) S31N-M2. (a) pH 5.9 VASGHD sample of W41F M2, showing chemical shift averaging (see projections at the top) at 298 K, which is absent at 273 K. The chemical shift difference indicates an exchange rate of ~400 s^{-1}, which can be attributed to exchange between the conformations of highly charged (+3 and +4) tetrads. (b) pH 5.5 VAGLI sample of W41F M2, showing 2D exchange cross peaks at 308 K but not at 273 K. These indicate motions on the hundreds of milliseconds timescale, which can be attributed to conformational motions in less highly charged tetrads. 1D cross sections are shown to indicate the X-Y exchange cross peaks. (c) pH 5.5 VASGHD sample with bound Amt sample. Drug binding arrests the conformational interconversion. (d) S31N M2, which has the intact HxxxW motif, shows L38 Cβ chemical shift averaging between the X and Y states at high temperature.

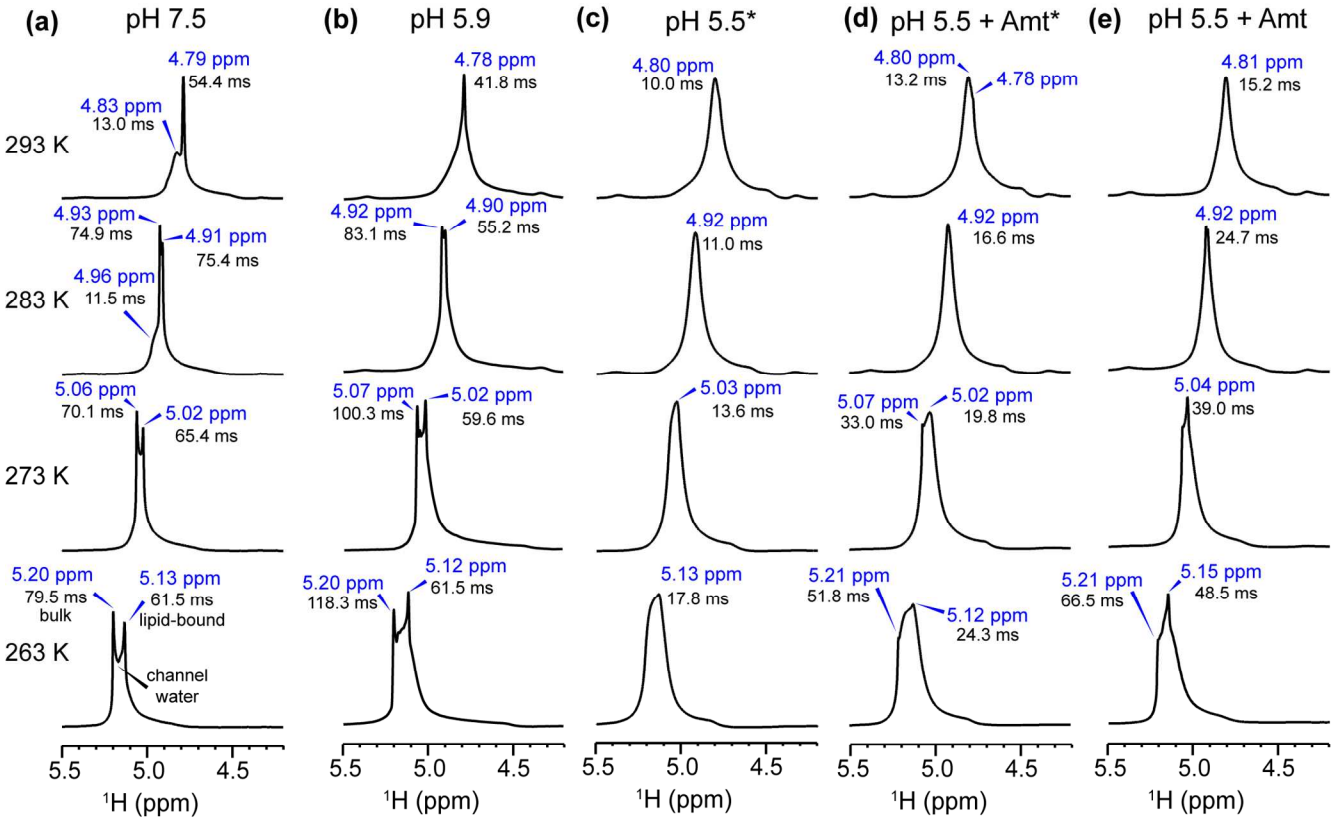

Figure 5. Water ^{1}H MAS spectra of membrane-bound VASGHD and VAGLI(*)-labeled W41F M2TM from 293 K to 263 K. (a) pH 7.5. (b) pH 5.9. (c) pH 5.5. (d) pH 5.5 with amantadine. (e) pH 5.5 with Amt. The spectra in (c) and (d) were measured on the VAGLI-labeled peptides while the other spectra were measured on the VASGHD-labeled peptides. The spectra were measured at 800 MHz under 11 kHz MAS. Two water peaks are resolved at high pH at low temperature, but are averaged at and below pH 5.5, indicating chemical exchange.

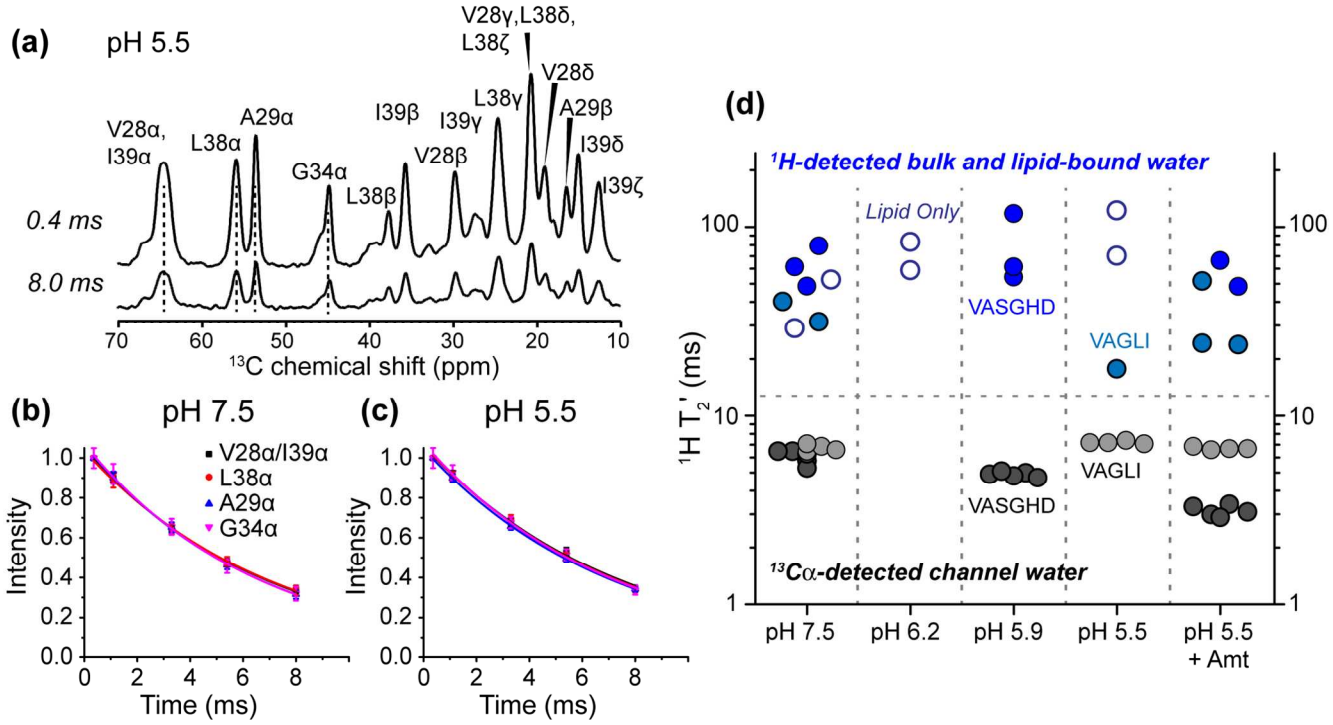

Figure 6. ^{13}C-detected water ^{1}H T_2 indicate slow dynamics of the channel water. (a) Representative ^{13}C MAS spectra after ^{1}H polarization transfer from water. The spectra of the pH 5.5 sample were measured with ^{1}H echo delays of 0.4 and 8.0 ms. (b-c) ^{13}C-detected water ^{1}H T_2 relaxation decay curves of the (b) pH 7.5 and (c) pH 5.5 samples. (d) Summary of water ^{1}H T_2's at 263 K detected by ^{1}H (*blue*) and ^{13}C (*black*). The ^{13}C-detected channel water T_2 relaxation times are an order of magnitude shorter than the ^{1}H-detected bulk and lipid-bound water.

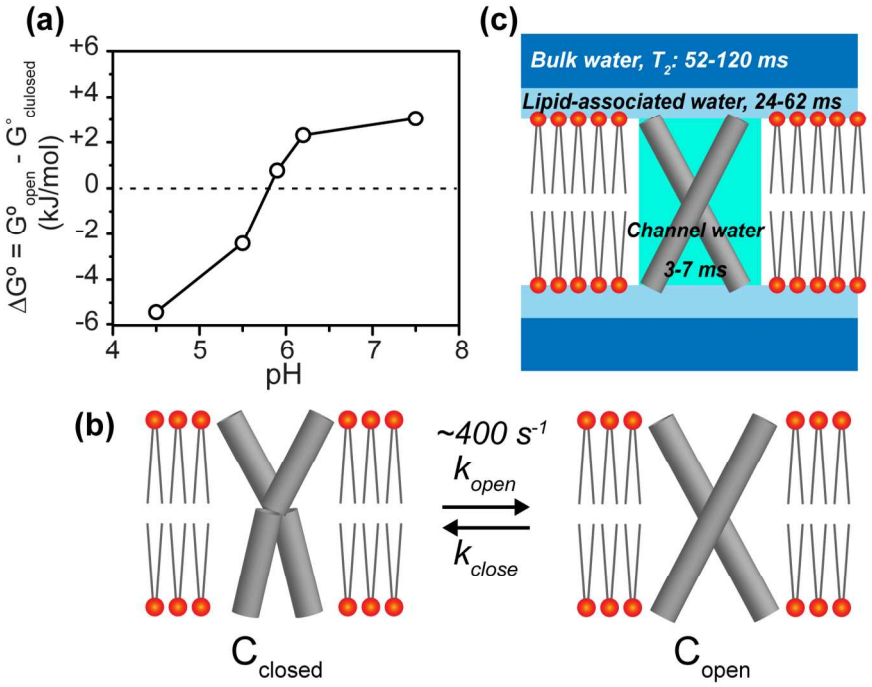

Figure 7. M2TM conformational dynamics and channel water dynamics. (a) Free energy difference ($\Delta G°$) between the C_{open} and C_{closed} conformations as a function of pH. The two states have equal energies at pH 5.8. (b) Schematic of the two tetramer conformations, which interconvert at ~ 400 s^{-1} at pH 5.9 and 298 K. (c) ^1H T_2 relaxation times of water pools in membrane-bound M2TM, measured at 263 K. The channel water exhibits ^1H T_2 values that are an order of magnitude shorter than the T_2's of lipid-associated water and bulk water.

References

(1) Hille, B. *Ionic channels of excitable membranes*; 2nd ed.; Sinauer Associates Inc.: Sundeland, 1992.

(2) Pinto, L. H.; Lamb, R. A. *J. Biol. Chem.* **2006**, *281*, 8997-9000.

(3) Cady, S. D.; Luo, W. B.; Hu, F. H.; Hong, M. *Biochemistry* **2009**, *48*, 7356-7364.

(4) Hong, M.; DeGrado, W. F. *Protein Sci.* **2012**, *21*, 1620-1633.

(5) Wang, C.; Lamb, R. A.; Pinto, L. H. *Biophys. J.* **1995**, *69*, 1363-1371.

(6) Balannik, V.; Carnevale, V.; Fiorin, G.; Levine, B. G.; Lamb, R. A.; Klein, M. L.; Degrado, W. F.; Pinto, L. H. *Biochemistry* **2010**, *49*, 696-708.

(7) Tang, Y.; Zaitseva, F.; Lamb, R. A.; Pinto, L. H. *J. Biol. Chem.* **2002**, *277*, 39880-39886.

(8) Ma, C. L.; Fiorin, G.; Carnevale, V.; Wang, J.; Lamb, R. A.; Klein, M. L.; Wu, Y. B.; Pinto, L. H.; DeGrado, W. F. *Structure* **2013**, *21*, 2033-2041.

(9) Wang, J.; Qiu, J. X.; Soto, C. S.; DeGrado, W. F. *Curr. Opin. Struct. Biol.* **2011**, *21*, 68-80.

(10) Hu, F.; Schmidt-Rohr, K.; Hong, M. *J. Am. Chem. Soc.* **2012**, *134*, 3703-3713.

(11) Liao, S. Y.; Yang, Y.; Tietze, D.; Hong, M. *J. Am. Chem. Soc.* **2015**, *137*, 6067-6077.

(12) Williams, J. K.; Tietze, D.; Lee, M.; Wang, J.; Hong, M. *J. Am. Chem. Soc.* **2016**, *138*, 8143-8155.

(13) Hu, F.; Luo, W.; Hong, M. *Science* **2010**, *330*, 505-508.

(14) Williams, J. K.; Tietze, D.; Wang, J.; Wu, Y.; DeGrado, W. F.; Hong, M. *J. Am. Chem. Soc.* **2013**, *135*, 9885-9897.

(15) Hong, M.; Fritzsching, K. J.; Williams, J. K. *J. Am. Chem. Soc.* **2012**, *134*, 14753-14755.

(16) Mandala, V. S.; Liao, S. Y.; Kwon, B.; Hong, M. *J. Mol. Biol.* **2017**, *429*, 2192-2210.

(17) Acharya, A.; Carnevale, V.; Fiorin, G.; Levine, B. G.; Polishchuk, A.; Balannick, V.; Samish, I.; Lamb, R. A.; Pinto, L. H.; DeGrado, W. F.; Klein, M. L. *Proc. Natl. Acad. Sci. U. S. A.* **2010**, *107*, 15075-15080.

(18) Sharma, M.; Yi, M.; Dong, H.; Qin, H.; Peterson, E.; Busath, D. D.; Zhou, H. X.; Cross, T. A. *Science* **2010**, *330*, 509-512.

(19) Hu, J.; Fu, R.; Nishimura, K.; Zhang, L.; Zhou, H. X.; Busath, D. D.; Vijayvergiya, V.; Cross, T. A. *Proc. Natl. Acad. Sci. USA* **2006**, *103*, 6865-6870.

(20) Williams, J. K.; Zhang, Y.; Schmidt-Rohr, K.; Hong, M. *Biophys. J.* **2013**, *104*, 1698-1708.

(21) Liang, R.; Swanson, J. M.; Madsen, J. J.; Hong, M.; DeGrado, W. F.; Voth, G. A. *Proc. Natl. Acad. Sci. USA* **2016**, *113*, E6955–E6964.

(22) Cady, S. D.; Schmidt-Rohr, K.; Wang, J.; Soto, C. S.; Degrado, W. F.; Hong, M. *Nature* **2010**, *463*, 689-692.

(23) Cady, S. D.; Wang, J.; Wu, Y.; DeGrado, W. F.; Hong, M. *J. Am. Chem. Soc.* **2011**, *133*, 4274-4284.

(24) Wang, C.; Takeuchi, K.; Pinto, L. H.; Lamb, R. A. *J. Virol.* **1993**, *67*, 5585-5594.

(25) Hu, J.; Asbury, T.; Achuthan, S.; Li, C.; Bertram, R.; Quine, J. R.; Fu, R.; Cross, T. A. *Biophys. J.* **2007**, *92*, 4335-4343.

(26) Luo, W.; Hong, M. *J. Am. Chem. Soc.* **2010**, *132*, 2378-2384.

(27) Cady, S. D.; Hong, M. *Proc. Natl. Acad. Sci. U.S.A* **2008**, *105*, 1483-1488.

(28) Hu, F.; Luo, W.; Cady, S. D.; Hong, M. *Biochim. Biophys. Acta* **2011**, *1808*, 415-423.

(29) Cristian, L.; Lear, J. D.; DeGrado, W. F. *Proc. Natl. Acad. Sci. USA* **2003**, *100*, 14772-14777.

(30) Kim, S. S.; Upshur, M. A.; Saotome, K.; Sahu, I. D.; McCarrick, R. M.; Feix, J. B.; Lorigan, G. A.; Howard, K. P. *Biochemistry* **2015**, *54*, 7157-7167.

(31) Duong-Ly, K. C.; Nanda, V.; DeGrado, W. F.; Howard, K. P. *Protein Sci.* **2005**, *14*, 856-861.

(32) Saotome, K.; Duong-Ly, K. C.; Howard, K. P. *Biopolymers* **2015**, *104*, 405-411.

(33) Luo, W.; Cady, S. D.; Hong, M. *Biochemistry* **2009**, *48*, 6361-6368.

(34) Andreas, L. B.; Reese, M.; Eddy, M. T.; Gelev, V.; Ni, Q. Z.; Miller, E. A.; Emsley, L.; Pintacuda, G.; Chou, J. J.; Griffin, R. G. *J. Am. Chem. Soc.* **2015**, *137*, 14877-14886.

(35) Li, C.; Qin, H.; Gao, F. P.; Cross, T. A. *Biochim. Biophys. Acta* **2007**, *1768*, 3162-3170.

(36) Stouffer, A. L.; Acharya, R.; Salom, D.; Levine, A. S.; Di Costanzo, L.; Soto, C. S.; Tereshko, V.; Nanda, V.; Stayrook, S.; DeGrado, W. F. *Nature* **2008**, *451*, 596-599.

(37) Thomaston, J. L.; Alfonso-Prieto, M.; Woldeyes, R. A.; Fraser, J. S.; Klein, M. L.; Fiorin, G.; DeGrado, W. F. *Proc. Natl. Acad. Sci. USA* **2015**, *112*, 14260-14265.

(38) Khurana, E.; Dal Peraro, M.; DeVane, R.; Vemparala, S.; DeGrado, W. F.; Klein, M. L. *Proc. Natl. Acad. Sci. USA* **2009**, *106*, 1069-1074.

(39) Chen, W.; Huang, Y. D.; Shen, J. N. *J. Phys. Chem. Lett.* **2016**, *7*, 3961-3966.

(40) Lin, T. I.; Schroeder, C. *J. Virol.* **2001**, *75*, 3647-3656.

(41) Mould, J. A.; Drury, J. E.; Frings, S. M.; Kaupp, U. B.; Pekosz, A.; Lamb, R. A.; Pinto, L. H. *J. Biol. Chem.* **2000**, *275*, 31038-31050.

(42) Mould, J. A.; Li, H. C.; Dudlak, C. S.; Lear, J. D.; Pekosz, A.; Lamb, R. A.; Pinto, L. H. *J. Biol. Chem.* **2000**, *275*, 8592-8599.

(43) Jeong, B. S.; Dyer, R. B. *J. Am. Chem. Soc.* **2017**, *139*, 6621-6628.

(44) Williams, J. K.; Hong, M. *J. Magn. Reson.* **2014**, *247*, 118-127.

(45) Ghosh, A.; Qiu, J.; DeGrado, W. F.; Hochstrasser, R. M. *Proc. Natl. Acad. Sci. U. S. A.* **2011**, *108*, 6115-6120.

(46) Cady, S.; Wang, T.; Hong, M. *J. Am. Chem. Soc.* **2011**, *133*, 11572-11579.

(47) Huster, D.; Yao, X. L.; Hong, M. *J. Am. Chem. Soc.* **2002**, *124*, 874-883.

(48) Kwon, B.; Hong, M. *Biochemistry* **2016**, *55*, 5387-5397.

(49) Wang, T.; Cady, S. D.; Hong, M. *Biophys. J.* **2012**, *102*, 787-794.

(50) Wang, T.; Hong, M. *Biochemistry* **2015**, *54*, 2214-2226.

(51) Rossman, J. S.; Jing, X.; Leser, G. P.; Lamb, R. A. *Cell* **2010**, *142*, 902-913.

(52) Elkins, M. R.; Williams, J. K.; Gelenter, M. D.; Dai, P.; Kwon, B.; Sergeyev, I. V.; Pentelute, B. L.; Hong, M. *Proc. Natl. Acad. Sci. U. S. A.* **2017**, *114*, 12946-12951.

(53) Hsieh, C. H.; Sue, S. C.; Lyu, P. C.; Wu, W. G. *Biophys. J.* **1997**, *73*, 870-877.

(54) Tristram-Nagle, S.; Kim, D. J.; Akhunzada, N.; Kucerka, N.; Mathai, J. C.; Katsaras, J.; Zeidel, M.; Nagle, J. F. *Chem. Phys. Lipids* **2010**, *163*, 630-637.

(55) Böckmann, A.; Gardiennet, C.; Verel, R.; Hunkeler, A.; Loquet, A.; Pintacuda, G.; Emsley, L.; Meier, B. H.; Lesage, A. *J. Biomol. NMR* **2009**, *45*, 319-327.

(56) Wang, T.; Jo, H.; DeGrado, W. F.; Hong, M. *J. Am. Chem. Soc.* **2017**, *139*, 6242-6252.

(57) Kucerka, N.; Tristram-Nagle, S.; Nagle, J. F. *J. Membr. Biol.* **2005**, *208*, 193-202.

(58) Bloembergen, N.; Purcell, E. M.; Pound, R. V. *Phys. Rev.* **1948**, *73*, 679-712.

(59) Cady, S. D.; Goodman, C.; C.Tatko; DeGrado, W. F.; Hong, M. *J. Am. Chem. Soc.* **2007**, *129*, 5719-5729.

(60) Cady, S. D.; Hong, M. *J. Biomol. NMR* **2009**, *45*, 185-196.

(61) Cady, S. D.; Wang, T.; Hong, M. *J. Am. Chem. Soc.* **2011**, *133*, 11572-11579.

(62) Carnevale, V.; Fiorin, G.; Levine, B. G.; DeGrado, W. F.; Klein, M. L. *J. Phys. Chem. C* **2010**, *114*, 20856-20863.

(63) Chen, H.; Wu, Y.; Voth, G. A. *Biophys. J.* **2007**, *93*, 3470-3479.

(64) Khurana, E.; DeVane, R. H.; Peraro, M. D.; Klein, M. L. *Biochim. Biophys. Acta* **2011**, *1808*, 530-537.

TOC figure

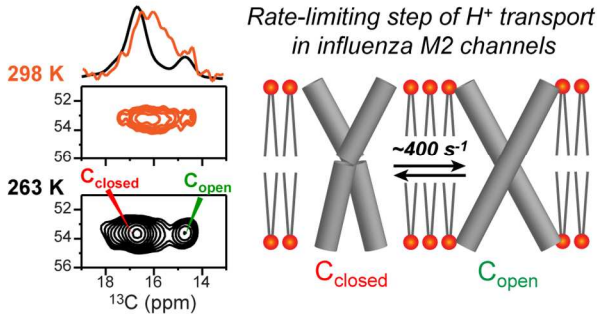
298 K
52
54
56
263 K
C_{closed}
C_{open}
52
54
56
18
16
14
^{13}C (ppm)
Rate-limiting step of H^+ transport
in influenza M2 channels
~400 s^{-1}
C_{closed}
C_{open}